Divergent Fields, Charge, and Capacitance in FDTD Simulations

Christopher L. Wagner and John B. Schneider, *Member, IEEE*

Abstract—**Finite-difference time-domain (FDTD) grids are often described as being divergence-free in a source-free region of space. However, in the presence of a source, the continuity equation states that charges may be deposited in the grid, while Gauss's law dictates that the fields must diverge from any deposited charge. The FDTD method will accurately predict the (diverging) fields associated with charges deposited by a source embedded in the grid. However, the behavior of the charge differs from that of charge in the physical world, unless the FDTD implementation is explicitly modified to include charge dynamics. Indeed, the way in which charge behaves in an FDTD grid naturally leads to the definition of grid capacitance. This grid capacitance, though small, is an intrinsic property of the grid and is independent of the way in which energy is introduced. To account for this grid capacitance, one should use a slightly modified form of the lumped-element capacitor model currently used.**

Index Terms—**FDTD methods.**

I. INTRODUCTION

IT IS WELL established that the finite-difference time-domain (FDTD) method can accurately model a wide range of wave propagation and scattering problems. There are, however, significant differences between the behavior of a system governed by finite-difference formulations of Maxwell's equations and one governed by the complete formulation of continuum physics. In the "discretized world," finite-difference calculus needs to be used to compute quantities, and the continuous forms are not directly applicable to data extracted from the grid [1]. Another distinction between the discretized FDTD world and the physical world is a by-product of the way in which the FDTD method is implemented. A typical FDTD simulation does not explicitly include charge dynamics and, thus, has properties not expected from the physics. For example, in an FDTD simulation, positive and negative charges can be deposited in free space and, though the fields associated with these charges are correct, the charges do not move and are, in a sense, infinitely massive.

In free-space regions in the absence of a source, the FDTD method can be shown to be divergence free [2], although the derivation of this property of the FDTD grid assumes infinite precision. In practice, FDTD simulations use finite
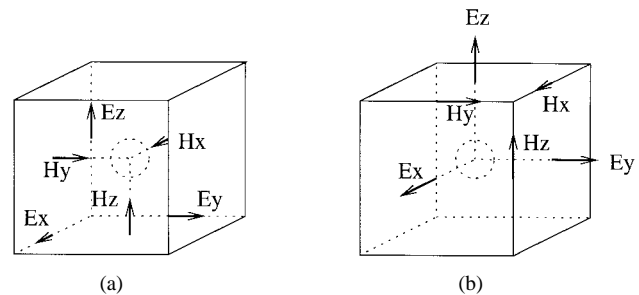
Fig. 1. Yee grid showing location of implicit magnetic or electric charge. (a) $\boldsymbol{H}$: centered-unit-cell magnetic charge. (b) $\boldsymbol{E}$: centered-unit-cell electric charge.

precision and, thus, the fields are not completely divergence free. However, the amount that fields diverge, representing a failure of charge conservation, is near the numeric noise floor of the simulation and is of little practical concern.

On the other hand, substantial field divergence can be (and, indeed, should be) produced by certain sources embedded in the computational domain. Current sources with a dc component can deposit persistent charges while current sources with no dc component can produce temporary charging. The geometry of the source, as well as the temporal form of the source function, ultimately dictates the amount of charging. Open-ended filamentary radiators can deposit charge because the current diverges at the ends. The charge is not represented by a separately stored quantity, but only by the divergence of a field.

The relationship between the electric field $\boldsymbol{E}$ and charge density ρ is given by Gauss's law

$$\epsilon_0 \nabla \cdot \boldsymbol{E} = \rho. \tag{1}$$

When the field diverges from a point, (1) states that the charge density is nonzero. The Yee space lattice staggers the field components in space to allow the spatial derivatives in Maxwell's equations to be computed with second-order accurate central differences. This arrangement of the field vector components also allows the divergence to be computed with central differences, thus preserving the second-order accuracy of charge-density computations. The charge density (field divergence) is, therefore, defined between the field vectors. The geometry of Yee-grid cells with implicit charge locations is shown in Fig. 1.

In the following section, the deposition of charge in an FDTD grid and the associated fields are examined. Both "harmonic" and transient sources are considered. Since the

FDTD grid can store charge, it is natural to define a grid capacitance. This capacitance is considered in Section III.

II. SOURCES AND CHARGING

In this section, the relationship between the currents, fields, and charge is examined using finite-difference calculus. Examples are given that show how charge may exist in the FDTD grid even though there is no explicit storage location for charge. Indeed, the charge "exists" only insofar as diverging fields exist. These diverging fields, which are required to satisfy the continuity equation, may persist indefinitely and, hence, remain in the computational domain even after all the radiated fields are gone.

The equations relevant to the discussion here are Maxwell's curl equations and the continuity equation

$$\epsilon_0 \frac{\partial \boldsymbol{E}}{\partial t} = \nabla \times \boldsymbol{H} - \boldsymbol{J} \qquad (2)$$

$$\mu_0 \frac{\partial \boldsymbol{H}}{\partial t} = -\nabla \times \boldsymbol{E} - \boldsymbol{M} \qquad (3)$$

$$\nabla \cdot \boldsymbol{J} = -\frac{\partial \rho}{\partial t}. \qquad (4)$$

A continuity equation similar to (4) governs the nonphysical magnetic currents and magnetic charges. Note that *any* function added to Ampere's law (2) [or Faraday's law (3)] is formally a current density $\boldsymbol{J}$ (or magnetic current density $\boldsymbol{M}$) and thus produces charge in accordance with the continuity equation. The FDTD currents are spatially collocated with the corresponding field components and offset a half-step in time. Thus, e.g., each component of $\boldsymbol{J}$ is collocated with the colinear component of $\boldsymbol{E}$, but is offset a half-step in time.

Consider a filamentary current source that consists of one or more elements. In accordance with the continuity equation, charge will exist at the ends of this source. The amount of charge at one end of the current source, i.e., the amount of charge enclosed within a surface surrounding the end of the filament, is given by the volume and temporal integration of (4)

$$-\int_{-\infty}^{t} \left[\oiint_S \boldsymbol{J} \cdot d\boldsymbol{s} \right] dt = \int_{-\infty}^{t} I(t)\, dt = Q_{\text{enc}} \qquad (5)$$

where $I(t)$ is the total current entering the volume and Q_{enc} is the enclosed charge. For an integrable source function, Q_{enc} can be determined analytically using continuum calculus. Alternatively, Q_{enc} can be determined in an FDTD simulation by the discrete-calculus volume integration of Gauss's law [1]. When the volume containing the charge is a single-cell cube with an edge length L, integration of (1) yields

$$\epsilon_0 \oiint_S \boldsymbol{E} \cdot d\boldsymbol{s} = \epsilon_0 L^2 \sum_{\text{six faces}} E_{\text{face}} = Q_{\text{enc}} \qquad (6)$$

where E_{face} is the total field on a face.

To illustrate the deposition of charge and to confirm the correspondence between the "expected" charge given by the temporal integral of the current and the "measured" charge obtained from the flux integral of the electric field, consider
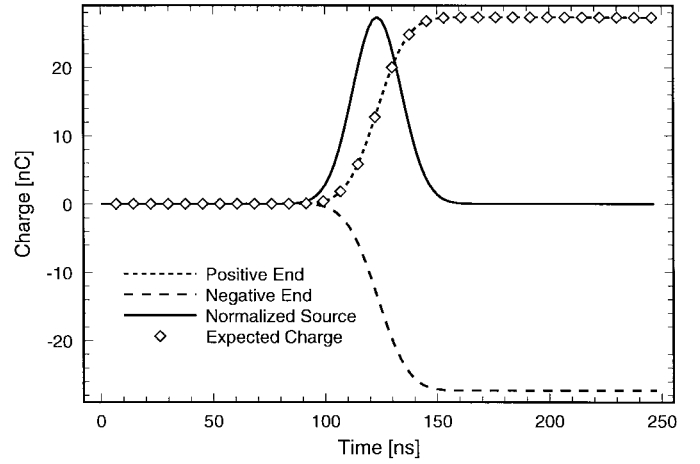

Fig. 2. Charge deposited at the ends of a dipole radiator versus time. The charge is "measured" from the FDTD grid using the finite-difference form of Gauss's law. The expected charge is computed from the time integral of the current waveform. For reference, the current source waveform is shown and is normalized to the peak expected charge. The actual peak current strength is 1 A.

a single-element current source driven by a Gaussian pulse. The charge as a function of time at the two ends of a single-element (Hertzian) current source is shown in Fig. 2. Results were obtained using an $81 \times 81 \times 81$ cubic cell domain with a 1-m cell spacing. (Note that the results shown in Fig. 2 are independent of this dimension, provided the current density is scaled to the grid size, i.e., the amount of charging is the same if the same $I(t)$ is used.) The current source was a single-element filament at grid coordinate (40, 40, 40) and a Higdon third-order absorbing boundary condition (ABC) was used to terminate the domain. Note that the measured FDTD results correspond precisely to those predicted by the temporal integral of the current. Thus, although the FDTD method is not considered a dc analysis technique, it does, nevertheless, properly predict the fields associated with the rearrangement of fixed (dc) charge.

A. Harmonic Sources

FDTD simulations sometimes employ "harmonic" sources. However, since a source must be turned on at some time, it is not truly harmonic. Consequently, the time integral of the current source function (i.e., the charge) can have a dc value. A specific example is a sinusoidal current, turned on at $t = 0$, which will deposit charge into the domain

$$\int_0^t I(t)\, dt = \int_0^t \sin(t)\, dt = 1 - \cos(t) = Q(t) \qquad (7)$$

where unit frequency and amplitude are used for simplicity. The charge oscillates between zero and two, and has an average value of one. This average charge which, for example, might be deposited at the ends of a Hertzian radiator, will produce nonzero dc fields throughout unshielded portions of the domain.

Cosine currents, turned on at $t = 0$, do not analytically deposit nonzero average charge. However, the large turn-on
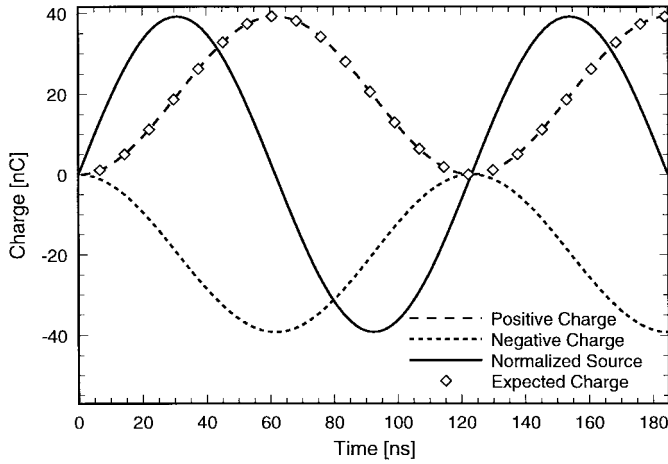
Fig. 3. Normalized source current and charge at ends of radiator versus time. The source is a sine wave turned on at $t = 0$ and the frequency is about 8.1 MHz. The charge at both ends of the radiator is computed from the divergence of $\boldsymbol{E}$. The charge has a nonzero average about which the instantaneous charge oscillates.
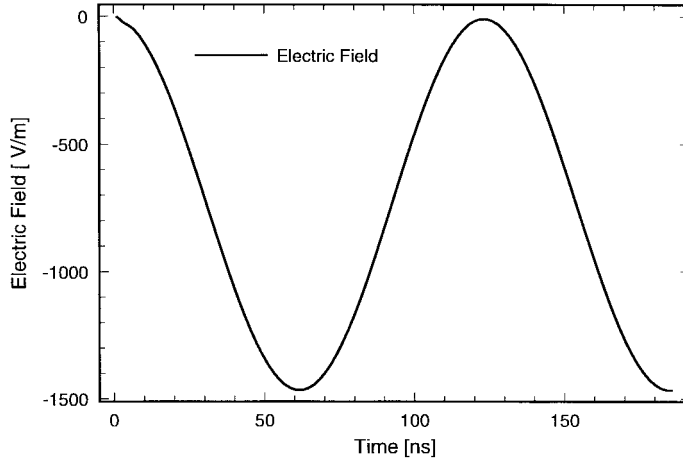

Fig. 4. Electric field at the radiator (between the charges) versus time. The same parameters are used as pertained to Fig. 3.

discontinuity of the cosine source function at $t = 0$ contains significant high-frequency components, which will suffer large numerical dispersion. In the analytic case, we have

$$\int_0^t I(t)\, dt = \int_0^t \cos(t)\, dt = \sin(t) = Q(t). \qquad (8)$$

The deposited charge $Q(t)$ oscillates between -1 and 1, with an average value of zero.

To demonstrate harmonic source charging, Fig. 3 shows the charge at the ends of a Hertzian radiator driven with a sinusoidal current that has a strength of 1 A and a period of 64 time steps (about 8.1 MHz). Fig. 4 shows the electric field at the radiator (between the charges). The domain for this example is the same as that used for Fig. 2. The nonzero mean in the charge and the electric field is a direct consequence of turning on the source at $t = 0$. These offsets are distinct from true harmonic solutions, which would have a zero mean.
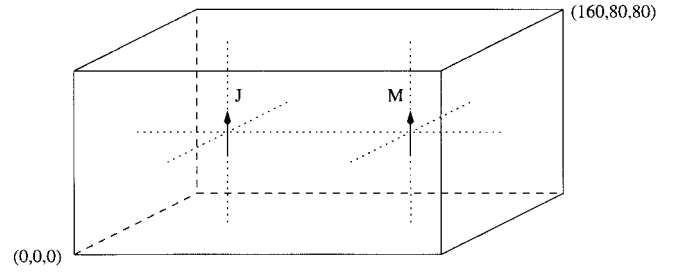

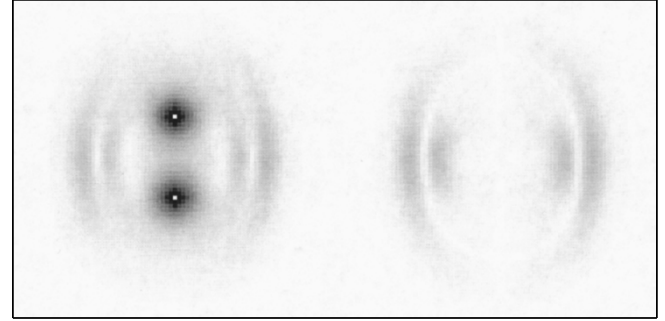Fig. 5. Domain geometry for electric/magnetic-charging example.

Fig. 6. Magnitude of $\boldsymbol{E}$ over a plane that includes the two sources. This snapshot was taken after 100 time steps. The electric-current source is to the left.

B. Transient Pulse Sources

Since the FDTD method is a time-domain technique, it is possible to compute the model response at several frequencies in a single run by using a transient source. As was shown in Fig. 2, if a Hertzian radiator consisting of a single element of electric current is driven by a pulse that has a nonzero dc component, then charge will be deposited into the domain. Here, the dc behavior of the fields in the vicinity of multielement radiators, driven either by electric or magnetic currents, is considered.

Consider the domain depicted in Fig. 5 of size $161 \times 81 \times 81$. This domain contains a z-directed 20-element-long electric current source centered at $40 \times 40 \times 40$ and a z-directed magnetic current source 20-elements long, centered at $120 \times 40 \times 40$. Magnetic charges and currents, while nonphysical, can be modeled in FDTD simulations as simply as electric charges and currents. The current on both sources is given by a Gaussian pulse. Early in the simulation, both of these sources have associated radiated fields, i.e., time-varying electric and magnetic fields that are coupled through Maxwell's equations. Figs. 6 and 7 show the magnitude of $\boldsymbol{E}$ and $\boldsymbol{H}$, respectively, measured over a plane that includes the source. A logarithmic grayscale is used to depict the fields where the darkness of a pixel is indicative of the field strength—the darker the pixel, the stronger the field. These figures show the radiated fields at a time when they are still close to their respective sources. Eventually, the radiated fields are absorbed by the ABC, and only the static fields due to the charges remain. As evidence of this, the electric-field magnitude is shown in Fig. 8 and the magnetic-field magnitude is shown in Fig. 9 at a time when the radiated fields have exited the computational space.
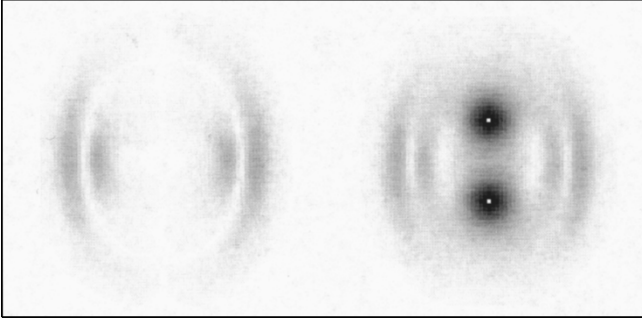
Fig. 7. Magnitude of H over a plane that includes the two sources. This snapshot was also taken after 100 time steps and is the dual of Fig. 6.
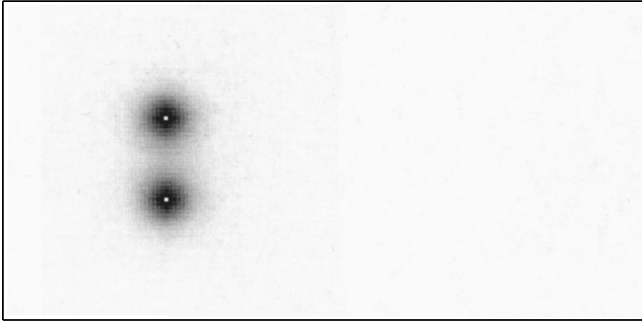

Fig. 8. Magnitude of E recorded after 300 time steps. The radiated field has left the domain and only the static fields (and charge) remain.
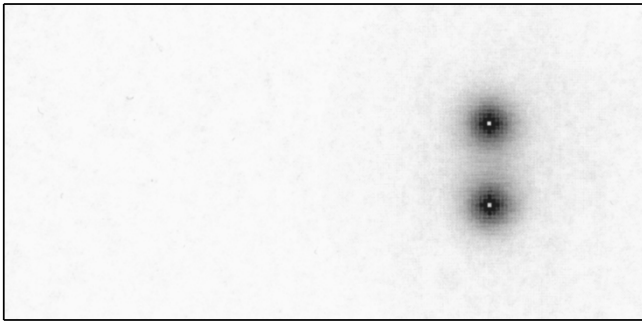

Fig. 9. Magnitude of H recorded after 300 time steps.

(The data in Figs. 6 and 8 have been normalized to the same value so that these figures can be compared qualitatively. The data in Figs. 7 and 9 have been similarly normalized.) The fields in Figs. 8 and 9 are static and purely divergent from the implied electric or magnetic charge at the ends of each source. Fig. 8 clearly shows that the electric-current source has deposited electric charge in the computational domain and, hence, perturbs the electric field. The perturbation is, of course, strongest near the deposited charge. On the other hand, the magnetic source does not deposit electric charge and, hence, does not affect the dc electric fields. Nevertheless, the magnetic source does, as shown in Fig. 9, deposit magnetic charge and does perturb the dc magnetic field. In these simulations, the Gaussian current pulse had a half-width (e^{-1}) of eight time steps ($\Delta t \approx 1.9 \times 10^{-9}$ s) and a peak of 1 A. The peak magnetic-current strength was 377 V/m^2 and the domain

boundaries were terminated with a third-order Higdon ABC applied to the tangential E-field components.

III. GRID CAPACITANCE

In the physical world, a positive and negative charge exert on each other an electrical force of attraction. In free space, these charges will move under the influence of this electrical force. In an FDTD model without charge dynamics, positive and negative charges in free space will not move. The charges are subject to coulomb forces, but no motion occurs. Consequently, since adjacent cells can store charge, it is natural to define a capacitance between cells of the grid.

The capacitance of adjacent cells in free space in the Yee grid can be derived in the following manner. The standard definition of capacitance is

$$C = Q/V \qquad (9)$$

where Q is the stored charge and V is the voltage between the charges. The charge stored in the grid can be found either from the temporal integral of the current that deposited the charge or from the finite-difference flux integral of E (Gauss's law). By expressing the charge in terms of the flux integral, an electric field appears in the numerator of (9), which can be cancelled with the electric field that subsequently appears in the denominator. When computing the flux integral, the total field at any point on the flux surface can be decomposed into two parts $E_{\text{face}} = E_{\text{enc}} + E_{\text{distant}}$. The contribution to the integral by the fields from "distant" sources (i.e., sources external to the surrounding surface) is zero. The field from the enclosed charge E_{enc} makes a nonzero contribution to the flux integral provided the total enclosed charge is nonzero. Consider a cubic-cell Gaussian surface that encloses a charge Q. The relationship between the charge and field on the faces of the cell surrounding the charge is from (6)

$$Q = \epsilon_0 L^2 \sum_{\text{six faces}} (E_{\text{enc}} + E_{\text{distant}}) = 6\epsilon_0 L^2 E_{\text{enc}} \qquad (10)$$

where L is the length of one side of the cubic cell. The expression on the right-hand side is a consequence of symmetry, which dictates that E_{enc} is the same over all six faces of a single-cell cube and of E_{distant} not contributing to the integral. The difference in potential between two adjacent cells containing charges of equal magnitude and opposite sign is

$$V = -\int_{\text{neg } Q}^{\text{pos } Q} E \cdot d\boldsymbol{l} = 2L E_{\text{enc}}. \qquad (11)$$

The factor of two is a consequence of the opposite charges doubling the total electric field over the face common to both cells. Using (10) and (11) in (9), the capacitance between adjacent nodes in the FDTD grid is found to be

$$C_{\text{grid}} = 3\epsilon_0 L. \qquad (12)$$

Thus, for example, the grid capacitance between adjacent nodes of a 1-m cubic unit cell will be about 26.6 pF.

To illustrate the effect of this grid capacitance and to verify (12), we discharge deposited charge through a conductance introduced into the grid. The rate of discharge is easily
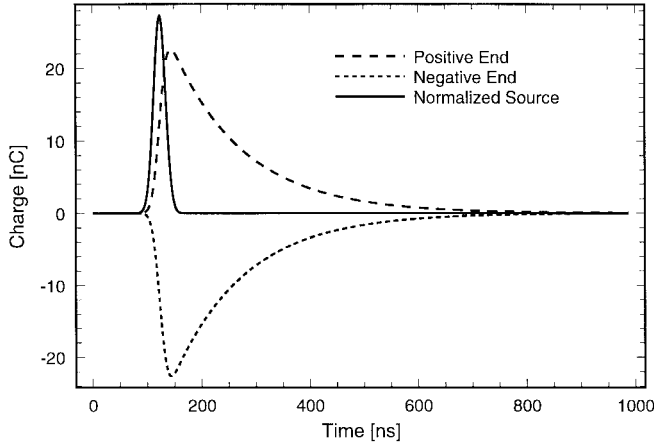
Fig. 10. Charge versus time when a conductivity is present. The same domain and source are used as in Fig. 2. The conductivity is $\sigma = 2 \times 10^{-4}$ S/m which is equivalent to 5 kΩ. The time constant which characterizes the discharge is 133 ns.

measured and can be used to obtain the associated time constant. From this time constant and the known resistance, one can obtain the capacitance. Charge deposited into the grid will discharge through conductance with a time constant

$$\tau = C_{\text{grid}} R_{\text{load}}$$

where R_{load} is the resistance associated with the conductivity at the grid location. Discharging of deposited charge is shown in Fig. 10. The grid spacing is 1 m with a load resistance of 5 kΩ [2] so the expected time constant, using the capacitance of (12), is 133 ns. The measured time constant which characterizes the decay shown in Fig. 10 is precisely this amount and, hence, verifies the capacitance predicted by (12).

We have only considered the capacity to store electric charge, but a similar (dual) effect exists for storage of magnetic charge. While it may be of theoretical or pedagogical interest to produce magnetic charge in a simulation, magnetic charge is not physical. Simulations which deposit magnetic charge (static or transient) are not modeling real-world electromagnetic problems. Nevertheless, magnetic sources that do not deposit magnetic charge, such as loops, may correspond to physical problems if the source is equivalent to an electric source.

When implementing lumped-element capacitors in an FDTD grid, the update equation at the location of the capacitor is modified to include the capacitive effects [3]. Previous formulations of lumped-elements have neglected the inherent grid capacitance. As described in [3], a lumped capacitor in a cubic-cell grid can be realized by changing the coefficients of the curl of the magnetic field. The new coefficient is

$$\frac{\Delta t/\epsilon_0}{1 + C_{\text{lump}}/(\epsilon_0 L)} \qquad (13)$$

where C_{lump} is the capacitance of the lumped element. Comparing this to the usual coefficient of $\Delta t/\epsilon_0$, one recognizes that the capacitor is realized, in essence, by using an effective permittivity ϵ_{eff} at a node. Equating $\Delta t/\epsilon_{\text{eff}}$ with (13) and solving for ϵ_{eff} yields

$$\epsilon_{\text{eff}} = \epsilon_0 + C_{\text{lump}}/L. \qquad (14)$$
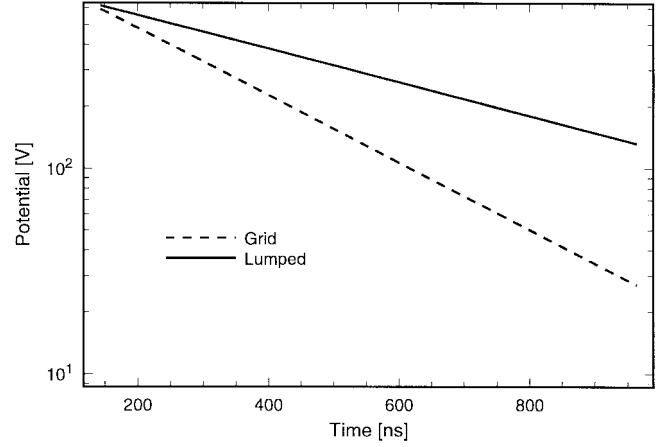

Fig. 11. Potential versus time when a conductivity is present. In one simulation, labeled "Grid," no additional capacitance is introduced so that only the inherent grid capacitance is present. In the other, labeled "Lumped," a lumped-element capacitor is introduced which has a capacitance equal to that of the inherent grid capacitance. Since inherent grid capacitance acts in parallel with the lumped-element capacitance, the time constant doubles. The plot shows the potential after the sources have been turned off. The strengths of the source functions were chosen so that curves were approximately equal when the sources were turned off (this has no effect on the time constants, but was done to facilitate interpretation of the plot).

However, since this effective permittivity does not account for the inherent grid capacitance, the total capacitance at the node will be larger than desired by the amount given by (12). When using (13), the total capacitance at that node is

$$C_{\text{lump}} + C_{\text{grid}} = L(\epsilon_{\text{eff}} - \epsilon_0) + 3\epsilon_0 L = L(\epsilon_{\text{eff}} + 2\epsilon_0). \quad (15)$$

Although one may have had the goal of introducing a capacitance of C_{lump} to the model, the total capacitance at that node will be $C_{\text{lump}} + C_{\text{grid}}$.

Fortunately, one can compensate for the inherent grid capacitance by subtracting the grid capacitance from the lumped capacitance in the calculation of the effective permittivity. Thus, to model a total capacitance C_{lump} at a given node, instead of (14), the effective permittivity should be

$$\epsilon'_{\text{eff}} = \epsilon_0 + (C_{\text{lump}} - C_{\text{grid}})/L = C_{\text{lump}}/L - 2\epsilon_0 \qquad (16)$$

where a prime has been added to distinguish this modified effective permittivity from the original. Alternatively, returning to the notation of [3], a modified form of the coefficient of the curl equation can be used to model a lumped-element capacitor C_{lump} provided one explicitly accounts for (i.e., subtracts) the additional grid capacitance. The correct coefficient is

$$\frac{\Delta t/\epsilon_0}{1 + (C_{\text{lump}} - C_{\text{grid}})/(\epsilon_0 L)} = \frac{\Delta t/\epsilon_0}{-2 + C_{\text{lump}}/(\epsilon_0 L)}. \quad (17)$$

Lumped capacitors with less than the grid capacitance (i.e., $C_{\text{lump}} < 3\epsilon_0 L$) cannot be implemented, as this would require reducing the permittivity to below ϵ_0. If smaller capacitors are required, the only option is to reduce the grid size so that the grid capacitance is less than the desired lumped capacitance.

A capacitor with a parallel-load resistor should discharge with a time constant of RC. In the FDTD grid, the total capacitance at a node is the sum of the lumped element and the inherent grid capacitance (15). To illustrate this point, Fig. 11 shows the potential, measured between charge locations, as a

function of time for two simulations. (The potential is indicative of the amount of charge present.) In the first simulation, deposited charge is discharged through a conductance and no lumped-element capactior is added, i.e., the only capacitance present is the inherent grid capacitance. In the second, a lumped-element capacitor with a capacitance equal to the inherent grid capacitance is introduced in accordance with the method described in [3]. Since the lumped element and inherent grid capacitance are equal, the addition of the lumped element doubles the time constant. Viewed another way, if one were to ignore the inherent grid capacitance, the time constant would be incorrect by a factor of two.

IV. CONCLUSIONS

Sources in the FDTD computational domain can deposit charge which produce dc offsets in the fields. The charge is evident by the divergence of the field. The field associated with deposited (static) charge is accurately predicted by the FDTD method in accordance with Gauss's law. However, because charge cannot move within the FDTD grid, there is an inherent grid capacitance, which is a function of the grid spacing. One can account for this grid capacitance when introducing lumped elements to obtain the desired capacitance.

REFERENCES

[1] W. C. Chew, "Electromagnetic theory on a lattice," *J. Appl. Phys.*, vol. 75, pp. 4843–4850, May 1994.

[2] A. Taflove, *Computational Electrodynamics: The Finite-Difference Time-Domain Method*. Norwood, MA: Artech House, 1995.

[3] M. Piket-May, A. Taflove, and J. Baron, "FDTD modeling of digital signal propagation in 3-D circuits with passive and active loads," *IEEE Trans. Microwave Theory Tech.*, vol. 42, pp. 1514–1523, Aug. 1994.

Christopher L. Wagner received the B.S. degree in physics and the B.S.E.E. degree from the University of Washington, Seattle, in 1979, and the M.S.E.E degree from Washington State University, Pullman, in 1998.

Upon graduation, he worked in research engineering, beginning at the Nuclear Physics Laboratory, University of Washington. He has also worked as a Consultant for several years for SAIC, Bellevue, WA. His recent work includes consulting for International Sensor Technology. He currently conducts research in computational electromagnetics and acoustics.

John B. Schneider (M'92) received the B.S. degree in electrical engineering *summa cum laude* from Tulane University, New Orleans, LA, and the M.S. and Ph.D. degrees in electrical engineering from the University of Washington, Seattle.

He is currently an Associate Professor in the School of Electrical Engineering and Computer Science, Washington State University, Pullman. His research interests include the use of computational methods to analyze acoustic, elastic, and electromagnetic-wave propagation.

Dr. Schneider received an Office of Naval Research Young Investigator Award in 1996.